Phenomenological theory of the reconstructive phase transition between the NaCl and CsCl structure types

P. Tolédano,* K. Knorr,† L. Ehm, and W. Depmeier
Universität Kiel, Institut für Geowissenschaften, Mineralogie/Kristallographie, Olshausenstrasse 40, D-24098 Kiel, Germany
(Received 19 November 2002; published 29 April 2003)

A phenomenological model of the reconstructive transformation between the NaCl and CsCl structure types is described. It consists of two consecutive displacive mechanisms, coupled to tensile and shear strains. These mechanisms give rise to intermediate orthorhombic structures, including the *B*16 and *B*33 structure types. The model is shown to explain consistently the experimental observations in different groups of binary compounds as monochalcogenides, monopnictides, and monohalides. The isostructural transitions found in rare-earth chalcogenides are interpreted by the coupling of the displacive order parameters to the change in compressibility related to the valence transitions. The previous models proposed for the NaCl-CsCl transformation are critically analyzed.

DOI: 10.1103/PhysRevB.67.144106 PACS number(s): 64.70.Kb, 81.30.Kf

I. INTRODUCTION

The current—phenomenological or statistical physics—approaches to phase transitions do not apply, in principle, to reconstructive structural phase transitions, because the absence of a group-subgroup relationship between the symmetries of the phases surrounding these transitions does not allow the definition of an order parameter, which is the preliminary step for the theoretical description of a phase transition. This traditional view was recently contradicted by a number of works[1–6] that, starting from the concrete analysis of the transition mechanisms of some reconstructive transitions, showed that the corresponding order parameters could be defined as nonlinear periodic functions of the critical degrees of freedom involved at the transitions (atomic displacements, spontaneous strains, probability of occupancy of selected positions by the atoms, etc.). In particular, it was shown that starting from a given structure, definite values of the critical variables could give rise to new symmetry operations associated with another structure, destroying the group-subgroup relationship with the initial structure. Most of the examples of reconstructive transitions, considered in Refs. 1–6, were taken among element crystals,[1–6] since the simplicity of their structures allows to demonstrate the connection between the transition order parameters and the critical displacements and ordering of the atoms more directly. The aim of the present work is to show, in the same framework, that a full theoretical treatment can be proposed for the reconstructive phase transition between the NaCl and CsCl type structures, which takes place in several families of binary compounds.

Various crystallogeometric models have been proposed for the transformation between the NaCl and CsCl structural types (denoted, respectively, *B*1 and *B*2) in reference to the experimental situation found in alkali and ammonium halides.[7–9] In these classes of ionic compounds, the *B*1 to *B*2 transition takes place directly on cooling or with increasing pressure and, due to the large volume change ranging from 10 to 17 %, has an explosive character, the crystal being generally broken into pieces in an almost polycrystalline state. Different orientational relationships were found for the *B*1 and *B*2 structures depending on the external conditions, on the samples sizes, etc., leading to the different proposed models, but no definite insight into the microscopic origin of the transition mechanism could be deduced from the experimental observations. In contrast, high pressure measurements on monochalcogenides[10–14] revealed that in these more covalently bonded compounds, the *B*1-*B*2 transition occurs with a volume change smaller than 5%, and often takes place via intermediate low-symmetry phases. These results shed light on the actual *B*1-*B*2 transformation path.

In the present work, the experimental data obtained for lead sulphide,[12–14] PbS are used to formulate a theoretical model of the *B*1-*B*2 transition (Sec. II). It is shown that this model explains the different and sometimes controversial observations reported for the *B*1-*B*2 transformation in other monochalcogenides, in monohalides, and in some pseudobinary compounds (Sec. III). At last (Sec. IV), the previous theoretical models of the *B*1-*B*2 transformation are critically analyzed.

II. THEORY OF THE *B*1-*B*2 PHASE TRANSFORMATION IN PbS

A. Structural mechanism for the *B*1-*B*33 transition

At room temperature and atmospheric pressure, PbS has the NaCl (*B*1) rock-salt structure (space group $Fm\bar{3}m$, $Z=1$). With increasing pressure a phase transition takes place at about 2.2 GPa to an orthorhombic phase having the TlI structure type (*B*33, $Cmcm$, $Z=4$).[14] The transition has a marked first-order character with a volume decrease of about 4.7%, and a wide region of coexistence between the *B*1 and *B*33 structures.[14] Furthermore, the reconstructive nature of the transition is typified by the absence of a simple group-subgroup relationship between the *B*1 and *B*33 symmetries, the coordination number of the Pb atoms increasing from 6 to 7, as shown in Figs. 1(a) and 1(b). X-ray observations indicate that the relationship between the basic vectors

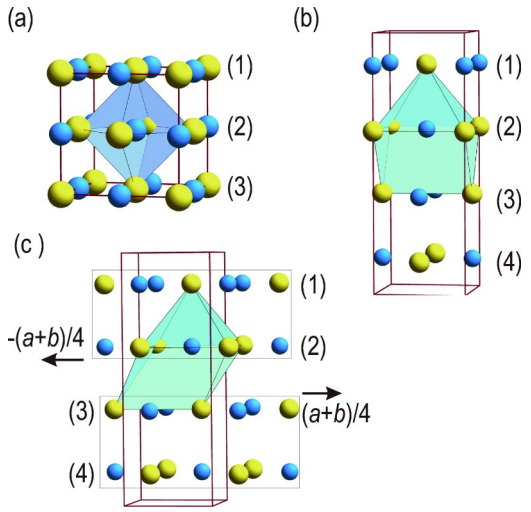

FIG. 1. Increase from 6 to 7 of the Pb coordination number when going from the $B1$ structure type (a) to the $B33$ structure type (b). (c) Displacive mechanism corresponding to the $B1$-$B16$-$B33$ mechanism. Comments on this figure are in the text.

$(\vec{a}_o,\vec{b}_o,\vec{c}_o)$ of the $B33$ orthorhombic unit cell and the basic vectors $(\vec{a},\vec{b},\vec{c})$ of the conventional face-centered cubic ($Z=4$) unit cell, is given by

$$\vec{a}_o=\frac{\vec{a}+\vec{b}}{2},\quad \vec{b}_o=2\vec{c},\quad \vec{c}_o=\frac{\vec{a}-\vec{b}}{2}. \tag{2.1}$$

The critical wave vector $\vec{k}_1$ of the fcc Brillouin zone associated with the change in translational symmetry expressed by Eq. (2.1), is $\vec{k}_1=(0,0,\pi/a)$. It is located at the middle of the Δ line, joining the center (Γ) to the boundary X point ($\vec{k}=(0,0,(2\pi)/a)$). $\vec{k}_1$ is invariant by the point-group $4mm$, and belongs to the six-branches star $\vec{k}_1^*$ with $\vec{k}_2=-\vec{k}_1,\vec{k}_3=(0,\pi/a,0),\vec{k}_4=-\vec{k}_3,\vec{k}_5=(\pi/a,0,0)$, and $\vec{k}_6=-\vec{k}_5$. Five irreducible representations (IR's) can, therefore, be constructed, which are labeled τ_1 to τ_5 in Kovalev's notation.[15] A standard Landau symmetry analysis shows that the twelve-dimensional IR $\tau_5(k_1^*)$ induces the $Pbnm$ space group for the equilibrium values $\eta_1=\eta_2=\eta\neq 0,\eta_3=\cdots=\eta_{12}=0$ of the corresponding twelve-component order parameter. It corresponds to the GeS-type ($B16$) structure having the same basic translations as the $B33$ primitive unit cell [Eq. (2.1)]. The displacive mechanism associated with the $B1\rightarrow B16$ phase transition, which represents the effective order-parameter components $\eta_1=\eta_2$, is shown in Fig. 1(c). It consists of an antiparallel shifting ξ of the atoms located in the (001) cubic bilayers, denoted (1,2) and (3,4) in Fig. 1(c), in the cubic directions $\pm[110]$. One can see from Fig. 1(c) that for the specific magnitude $\xi_c=-a/(4\sqrt{2})$, corresponding to the atomic displacement, $(\vec{a}+\vec{b})/4$, *the* $B16$ *structure becomes the* $B33$ *structure*, i.e., the $B33$ structure is formed for definite *critical* displacement ξ_c of the atoms from their initial cubic position in the $\pm[110]$ directions, and therefore represents a *limit state.* At the $B16$-$B33$ transition, the translational symmetry *increases*, since $Pbnm$ is a subgroup of index 2 of $Cmcm$. More precisely, the cell-doubling $B33$-$B16$ transition is induced by a one-dimensional IR (τ_7 or τ_8 in Kovalev's notation[15]) at the Y point $[k_c=(0,(2\pi)/b,0)]$ of the C centered orthorhombic Brillouin zone. This transition can be second-order.

B. Theory of the reconstructive $B1$-$B33$ transition

Let us formalize the mechanism described for the $B1$-$B33$ transition, using the procedure described in Ref. 1, by expressing the order-parameter amplitude η as a function of the atomic shifts ξ, taking into account the periodicity of the lattice in the $\pm[110]$ directions. One finds[16]

$$\eta(\xi)=\sin\left(\frac{2\pi\sqrt{2}}{a}\xi\right). \tag{2.2}$$

The $\eta(\xi)$ dependence is represented in Fig. 2(a). Thus for $\xi_c=0$ and $\xi_c=a/(2\sqrt{2})$, the B1 structure is formed, whereas for $\xi_c=a/(4\sqrt{2})$ and $\xi_c=3a/(4\sqrt{2})$, two different domains of the $B33$ structure occur, which can be deduced from one another by a fourfold rotation along the $\pm[110]$ directions. For all noncritical values of ξ, the $B16$ structure is obtained. The effective $\eta(\xi)$ expansion (Landau free energy), describing the phase diagram that involves the $B1$, $B16$, and $B33$, phases, is[17]

$$F[\eta(\xi)]=\frac{a}{2}\eta^2(\xi)+\frac{b}{4}\eta^4(\xi)+\frac{c}{6}\eta^6(\xi)+\cdots. \tag{2.3}$$

The equation of state results from the minimization of F with respect to the ξ variable

$$\frac{\partial\eta}{\partial\xi}=\eta(\xi)\frac{\partial\eta}{\partial\xi}[a+b\eta^2+c\eta^4+\cdots]=0. \tag{2.4}$$

It shows that there are the following three possible equilibrium structures:

(i) the $B1$ structure for $\eta(\xi)=0$, i.e., for $\xi_c=0,a/(2\sqrt{2}),a/(\sqrt{2}),\ldots$;

(ii) the $B33$ structure for $\partial\eta/\partial\xi=0$, for $\xi_c=a/(4\sqrt{2}),3a/(4\sqrt{2}),5a/(4\sqrt{2}),\ldots$;

(iii) the $B16$ structure for $a+b\eta^2+c\eta^4+\cdots=0$.

The region of stability for each of the three corresponding phases is determined by the inequality

$$\frac{\partial^2F}{\partial\xi^2}=\left[\left(\frac{\partial\eta}{\partial\xi}\right)^2+\eta\frac{\partial^2\eta}{\partial\xi^2}\right](a+b\eta^2+c\eta^4+\cdots)$$
$$+2\frac{\partial\eta}{\partial\xi}(b\eta+2c\eta^3+\cdots)\geqslant 0, \tag{2.5}$$

which yields the phase diagram represented in Fig. 2(b) in the plane $(a/c,b/c)$ of the phenomenological coefficients, where a and b are temperature- and pressure-dependent coefficients. The arrow in Fig. 2(b) figures the thermodynamic path followed for the reconstructive $B1$-$B33$ transition. Note that the three phases merge at the N point, and that the $B16$ phase can be reached from the $B1$ phase across a second- or

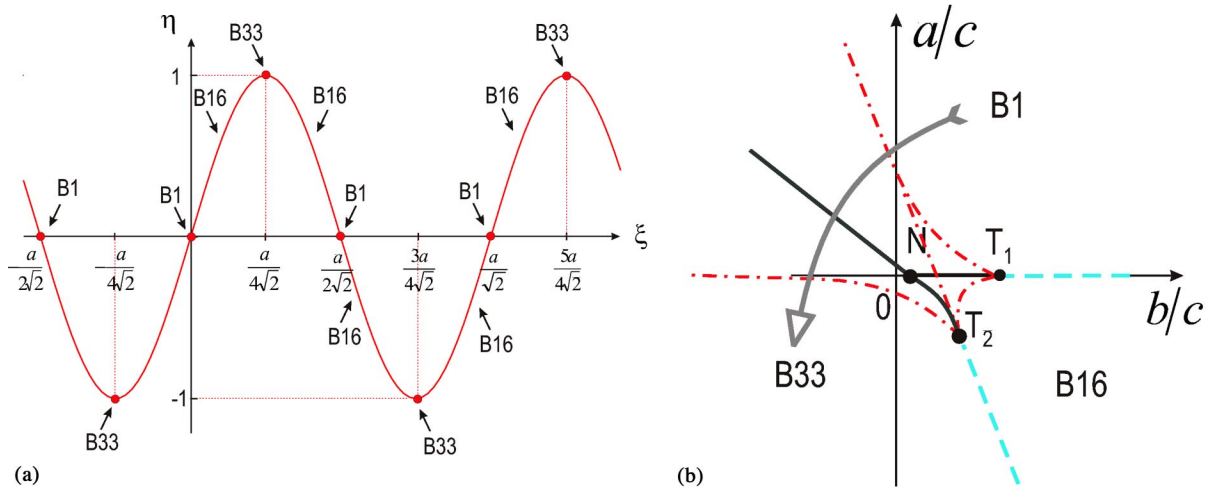

FIG. 2. (a) Sinusoidal dependence of the η order-parameter magnitude, associated with the $B1$-$B16$-$B33$ mechanism, on the atomic shifts ξ in the $\pm[110]$ directions, following Eq. (2.2). (b) Theoretical phase diagram corresponding to the Landau free energy defined by Eq. (2.3), in the $(a/c, b/c)$ plane. Solid lines are first-order transition lines. Dashed lines are second-order transition lines. Dashed-dotted lines are limit of stability lines enframing the first-order transition lines. N is a triple point. T_1 and T_2 are tricritical points. The arrow indicates the $B1$-$B33$ reconstructive transition path.

first-order transition line, the two regimes being separated by a tricritical point T_1. Another tricritical point T_2 is found on the line separating the $B16$ and $B33$ phases.

For a realistic description of the $B1$-$B33$ transition, one has to take into account, in addition to the primary (symmetry breaking) displacive order parameter η, the spontaneous strain components e_{xy} and $e=e_{xx}+e_{yy}-2e_{zz}$ associated with the $m\bar{3}m \rightarrow mmm_{xy}$ point-group change, which constitute secondary order parameters. The effective contribution of these strain components to the Landau free energy has the form[18]

$$F(\eta, e_{xy}, e) = \eta^2(\delta_1 e_{xy} + \delta_2 e) + \frac{d_1}{2} e_{xy}^2 + \frac{d_2}{2}\frac{e^2}{2}, \quad (2.6)$$

which denotes the improper ferroelastic character of the $B1$-$B33$ transition. Taking into account the values found[14] for the lattice parameters in the $B1$ ($a=5.9239$ Å) and $B33$ ($a_o=3.98$ Å, and $b_o=11.11$ Å, $c_o=4.16$ Å) structures yields: $e_{xy} \cong 0.006$ and $e \cong 0.1$, providing an estimate of the orthorhombic deformation of the initial cubic cell.

C. Structural mechanism for the $B33$-$B2$ reconstructive transition

Above about 22 GPa, PbS undergoes another first-order transition from the $B33$ structure to the primitive cubic CsCl ($B2$) type structure ($Pm\bar{3}m, Z=1$). The corresponding volume drop is $\sim 6\%$ at 22 GPa.[19] The reconstructive character of the $B33$-$B2$ transition is reflected by the absence of a group-subgroup relationship between the symmetries of the phases and by the increase of the coordination number for the Pb atoms from 7 to 8. Figures 3(a) and 3(b) represent our proposed transformation mechanism for this transition, which can be decomposed in the following two successive steps:

(i) A shifting of the atoms belonging to the layers denoted 1 and 4 in the $B33$ structure, in the same [110] direction, whereas the layers 2 and 3 remain unshifted. Figure 3(a) shows that for a general magnitude ξ' of the atomic shifts, the $Cmcm$ symmetry is lowered to its subgroup $Pbcm$ ($Z=4$), but for a displacement $(\vec{a}+\vec{b})/4$ of the atoms from their initial positions, the symmetry becomes $Cmmm$ ($Z=2$) with the basic vectors

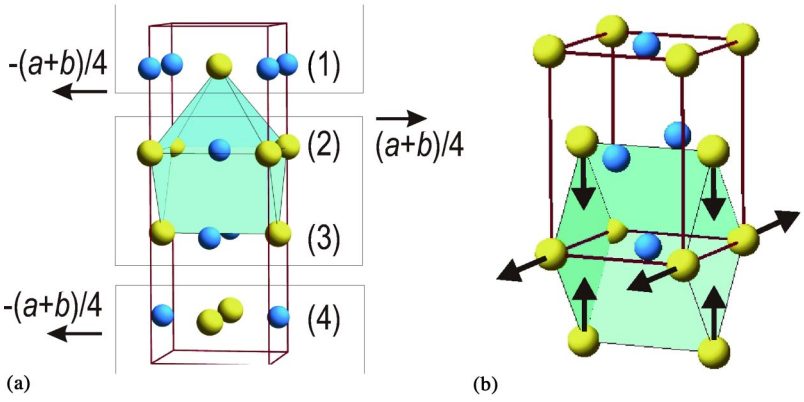

FIG. 3. (a) Atomic shifts, involving four (100) layers, from the $B33$-type structure to the $Pbcm$ intermediate symmetry and the $Cmmm$ limit phase, shown in (b). The $Cmmm$ unit cell is used for representing in (b) the atomic shifts corresponding to the shear strain e_{xy} at the $Cmmm \rightarrow Pm\bar{3}m$ ($B2$) transition. Comments on (a) and (b) are in the text.

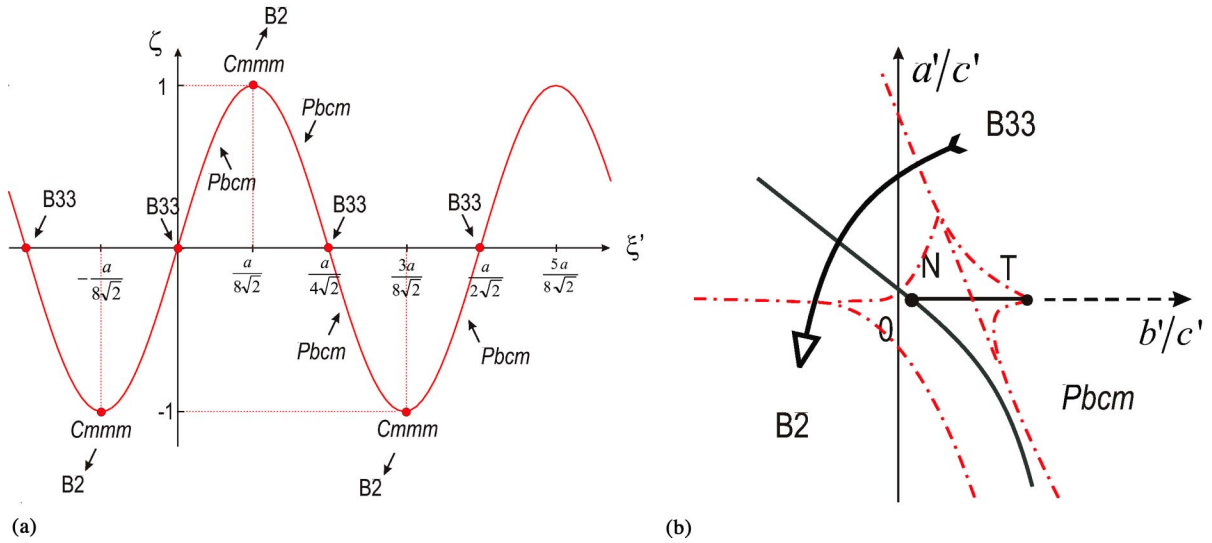

FIG. 4. (a) Sinusoidal dependence of the ζ order parameter in function of the atomic shifts in the $\pm[110]$ directions, following Eq. (2.9), and corresponding to the $Cmcm \rightarrow Pbcm \rightarrow Cmmm$ phase sequence. (b) Phase diagram associated with the Landau free energy defined by Eq. (2.10), in the $(a'/c', b'/c')$ plane. The $Cmmm$ phase is replaced by its shear-deformed $B2$ phase. The arrow indicates the reconstructive $B33$-$B2$ transition path.

$$\vec{a}_o' = \vec{a}_o, \quad \vec{b}_o' = \frac{\vec{b}_o}{2}, \quad \vec{c}_o' = \vec{c}_o. \tag{2.7}$$

The $Cmcm \rightarrow Pbcm \rightarrow Cmmm$ sequence of symmetries can be described analogously by an antiparallel shifting mechanism in the directions $\pm[110]$, the atoms belonging to the layers (1,4) and (2,3) being shifted in opposite directions. In this case the $Cmmm$ symmetry is formed for the critical shifting $\xi_c' = a/(8\sqrt{2})$ corresponding to the displacements $\pm(\vec{a}+\vec{b})/8$ of the atoms from their initial ($Cmcm$) positions. Note also that at the $Pbcm \rightarrow Cmmm$ transition, the translational symmetry increases, since $Pbcm$ is a subgroup of index 4 of $Cmmm$. The cell-quadrupling transition $Cmmm \rightarrow Pbcm$ is associated with a two-component order-parameter that has the symmetry of the two-dimensional IR τ_1 at the wave vector $k_c = (0, \pi/a, 0)$, located inside the C-centered orthorhombic Brillouin zone, at the middle of the ΓY segment (the Δ line).

(ii) The orthorhombic limit state with $Cmmm$ symmetry corresponds to a shear deformed $B2$ structure, i.e., it can be transformed into the $B2$ structure (to which it is group-subgroup related) by the shear strain e_{xy}. Figure 3(b) shows the displacive mechanism associated with the increase in symmetry from $Cmmm$ to $Pm\bar{3}m$. It involves three successive fcc layers forming the orthorhombic structure, and consists of a displacement of the atoms belonging to the first and third layers along the [001] direction, while the atoms of the intermediate layer 2, relax along the [110] direction. The relationship between the primitive cubic $(\vec{a}_c, \vec{b}_c, \vec{c}_c)$ and orthorhombic basic vectors $(\vec{a}_o, \vec{b}_o, \vec{c}_o)$ is

$$\vec{a}_o = \vec{a}_c, \quad \vec{b}_o = 2(\vec{b}_c + \vec{c}_c), \quad \vec{c}_o = -\vec{b}_c + \vec{c}_c. \tag{2.8}$$

D. Theory of the $B33$-$B2$ reconstructive transition

The $B33$-$B2$ transition follows the same theoretical scheme as the $B1 \rightarrow B33$ transition. Starting from the initial $B33$ structure, one gets the $Pbcm$ symmetry for a general magnitude of the atomic shifts ξ' in the $\pm[110]$ directions while the $Cmmm$ limit state is obtained for the critical shifts $\xi_c' = a/(8\sqrt{2})$. The $Cmcm \rightarrow Pbcm$ symmetry change is induced by a one-dimensional IR (τ_6 in Kovalev's notation [15]) at the Y point $(\vec{k}_1 = 0, 2\pi/b, 0)$ of the C-orthorhombic Brillouin zone. The corresponding single order-parameter component ζ can be expressed as a function of the antiparallel displacements ξ' [20]

$$\zeta(\xi') = \sin\left(\frac{4\pi\sqrt{2}}{a}\xi'\right), \tag{2.9}$$

which is represented in Fig. 4(a). Thus for $\xi_c' = 0, a/(4\sqrt{2}), a/(2\sqrt{2}), \ldots$, the $B33$ structure is formed, whereas for $\xi_c' = a/(8\sqrt{2}), 3a/(8\sqrt{2}), 5a/(8\sqrt{2}), \ldots$, the $Cmmm$ symmetry is obtained. For all other values of ξ', the $Pbcm$ symmetry occurs. The effective $\zeta(\xi')$ expansion is here

$$F'[\zeta(\xi')] = \frac{a'}{2}\zeta^2(\xi') + \frac{b'}{4}\zeta^4(\xi') + \frac{c'}{6}\zeta^6(\xi') + \cdots, \tag{2.10}$$

which by minimization with respect to ξ' yields the phase diagram represented in Fig. 4(b). In this phase diagram, the $Cmmm$ phase has been replaced by its shear-deformed cubic $B2$ transform. Since the shear strain e_{xy} always arises discontinuously at the $Pm\bar{3}m \rightarrow Cmmm$ transition, due to the existence of a cubic invariant $(e_{xy})^3$ in the corresponding free energy,[21] the transition separating the $Pbcm$ and $Pm\bar{3}m$

(a)

$$\begin{array}{ccccccccccc} \text{B1} & & \text{B16} & & \text{B33} & & Pbcm & & Cmmm & & \text{B2} \\ Fm\bar{3}m & \xrightarrow[\Delta]{(0,\pi/a,0)} & Pbnm & \xrightarrow[\text{Y}]{(0,(2\pi)/b,0)} & Cmcm & \xleftarrow[\text{Y}]{(0,(2\pi)/b,0)} & Pbcm & \xleftarrow[\Delta]{(0,\pi/b,0)} & Cmmm & \xleftarrow[\Gamma]{(0,0,0)} & Pm\bar{3}m \\ \text{V} & & 4\text{V} & & 4\text{V} & & 4\text{V} & & 2\text{V} & & \text{V} \end{array}$$

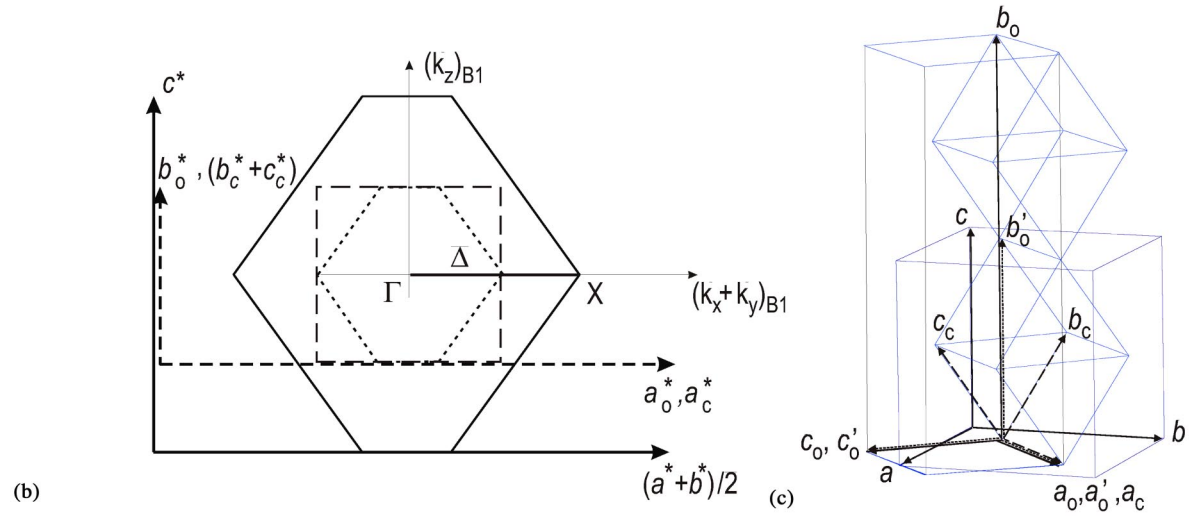

FIG. 5. (a) Symmetry connections between the structures involved in the $B1$-$B2$ transformation mechanism. It shows that the phonon instabilities occur on the same Δ direction of the fcc, primitive cubic and C-centered orthorhombic Brillouin zones. The volumes refer to the primitive unit cells. (b) Embedded $B1$ (full line), $B2$ (dashed), and $B33$ (dotted) projected Brillouin zones showing the coincidence of the respective Δ lines when the $B1$-$B2$ mechanism it taken into account. (c) Respective orientations of the lattices, as resulting from the proposed $B1$-$B2$ transformation mechanism. For labeling see text, Eqs. (2.1), (2.7), (2.8), and (2.11). [Note that the (c) reflects the $Ammm$ unit cell instead of the $Cmmm$ standard setting.)

phases is always first order. Note that the $Cmmm \rightarrow Pm\bar{3}m$ transition also requires the existence of the (improper) tensile strain component $e = e_{xx} + e_{yy} - 2e_{zz}$ as a secondary order parameter. Using the value found for the cubic lattice parameter in the $B2$ structure of PbS by Chattopadhyay *et al.*[19] ($a_c = 3.289$ Å) gives an estimate of $e_{xy} \cong 0.25$ and $e \cong 0.28$ at the $B33$-$B2$ transition.

E. The $B1$-$B2$ transformation mechanism in PbS

In summary, the $B1$-$B2$ transformation in PbS occurs via the intermediate ($B33$) orthorhombic phase having a wide region of stability ranging from 2.2 GPa to more than 35 GPa. The first-order transitions $B1$-$B33$ and $B33$-$B2$, which take place, respectively, at about 2.3 GPa and 22.5 GPa, can be described as displacive transitions of the reconstructive type. The $B33$ and $Cmmm$ phases correspond to limit states that are formed for critical displacement, and definite (primary or secondary) shear (e_{xy}) and tensile (e) strains. In these states, the translational symmetry increases with respect to the $B16$ and $Pbcm$ intermediate states, and the group-subgroup relationship with the initial structure (respectively $B1$ and $B33$) is lost. Figure 5(a) shows the symmetry connections occurring in the sequence of structures assumed in our model between the $B1$ and $B2$ phases. Using Fig. 5(b), which shows the embedding of the $B1$, $B33$, and $B2$ Brillouin zones, one can see from Fig. 5(a) that the successive transition mechanisms relate to the same Δ line, ΓX cubic or ΓY orthorhombic, of the Brillouin zones. The respective orientations of the $B1$ and $B2$ unit cells are represented in Fig. 5(c). It corresponds to the following relationships between the lattice vectors

$$\vec{a} = \vec{a}_c + \vec{b}_c - \vec{c}_c, \quad \vec{b} = \vec{a}_c - \vec{b}_c + \vec{c}_c, \quad \vec{c} = \vec{b}_c + \vec{c}_c, \tag{2.11}$$

which yield definite coincidences between the crystallographic directions in the $B1$ and $B2$ structures. They will be discussed in Sec. III C in light of the experimental observations in alkali halides.

The periodic (nonlinear) character of the displacive order parameters $\eta(\xi)$ and $\zeta(\xi')$ associated with the $B1$-$B33$ and $B33$-$B2$ transitions is summarized in Fig. 6(a). Note in this respect that these transitions involve different sequences of atomic layers, i.e., distinct displacive mechanisms, although the atoms are shifted in the same $\pm[110]$ directions. This is because the shearing required for obtaining the $B2$ structure occurs within the double layers, through a $b_o/2$ shift, which destroys the collective displacement of bilayers associated with the $B1$-$B33$ mechanism.

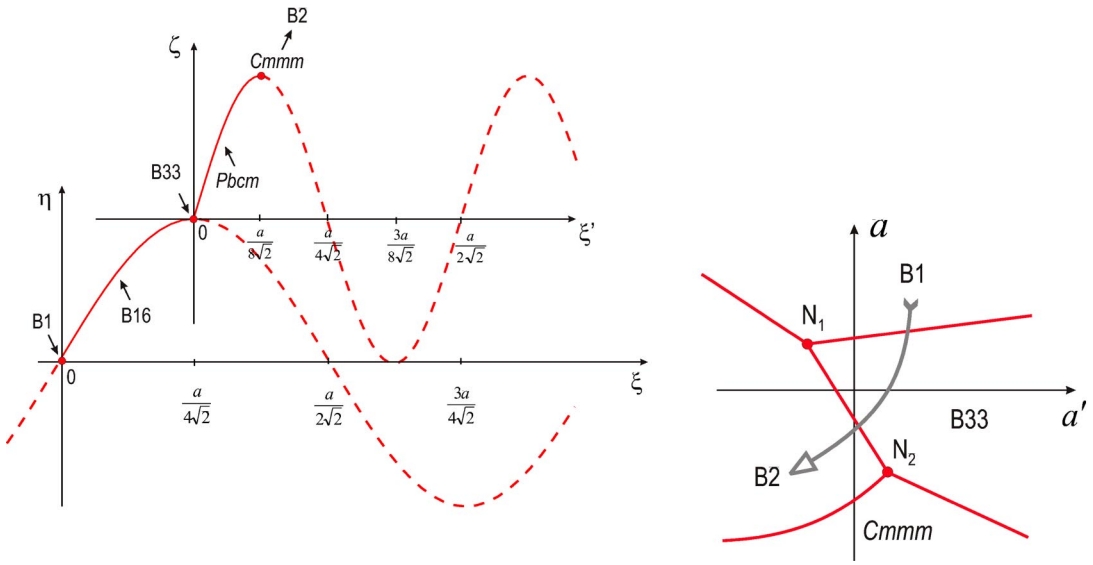

(a) (b)

FIG. 6. (a) Sinusoidal character of $B1$-$B2$ transition order parameters $\eta(\xi)$ and $\zeta(\xi')$. The solid curve shows the actual nonlinear dependence of the effective order parameter as a function of ξ and ξ'. Note that the $\eta(\xi)$ period is twice the $\zeta(\xi')$ period. (b) Phase diagram associated with the total free energy $F(\eta,\zeta)$ defined by Eq. (2.12). Comments on this figure are in the text. The lines and points have the same meaning as in Fig. 2(b). The arrow indicates the thermodynamic path followed in PbS.

Figure 6(b) shows schematically the topology of the phase diagram which contains only the $B1$ and $B2$; and intermediate limit phases of symmetries $Cmcm$ and $Cmmm$. It is obtained by minimizing the total free energy

$$F[\eta(\xi),\zeta(\xi')]=F[\eta(\xi)]+F'[\zeta(\xi')]+\delta\eta^2(\xi)\zeta^2(\xi'), \tag{2.12}$$

with respects to ξ and ξ', assuming large negative values for the coefficients b and b' ($b<-2\sqrt{a\gamma}$, $b'<-2\sqrt{a'\gamma'}$), so that the $B16$ and $Pbcm$ phases are unstable. The δ term expresses the coupling between the two displacive mechanisms which influences the $Cmcm$ intermediate region. The arrow in Fig. 6(b) indicates the thermodynamic path followed in PbS, but one can have a direct $B1$-$B2$ reconstructive transformation, since the $B1$, $B2$, and $B33$ phases merge at a triple point N_1. Note that, with the exception of the $Pm\bar{3}m\rightarrow Cmmm$ first-order transition line, all the transition lines in the phase diagram are straight lines as they represent reconstructive transitions.[22] Finally, it should be emphasized that our proposed transformation mechanism is fully reversible, i.e., although the $B1$ structure was taken in our description to be the ''parent'' structure, since it is stable at high temperature and low pressure, the $B2$ structure may be taken alternately as the initial parent structure by simply inverting the signs of the critical shifts and spontaneous strains.

III. APPLICABILITY OF THE MODEL

The $B1$-$B2$ transformation corresponds to the most widespreaded reconstructive mechanism found among binary compounds. Tables I to IV give an extensive list of materials in which the transformation has been observed. The majority of them belong to the classes of monochalcogenides and monohalides. In this section, we show that a consistent interpretation of the experimental results reported for the $B1$-$B2$ transformation can be made in light of our proposed model.

A. (Ge, Sn, Pb) and (Ca, Sr, Ba) chalcogenides

Monochalcogenides of the groups IV and II elements, which undergo a temperature- or pressure-induced $B1$-$B2$ transformation, are listed in Table I. PbSe displays the same $B1$-$B33$-$B2$ sequence of phases as PbS with similar volume drops at the $B1$-$B33$ and $B33$-$B2$ transitions. At variance, PbTe and SnTe show the $B16$ intermediate structure type assumed in our model to correspond to noncritical atomic shifts in the $\pm[110]$ directions. In our description, the group-subgroup related $B1$-$B16$ transition can take place continuously. This is verified in SnS and SnSe and to some extent in PbTe, GeTe, and SnTe where the drop in volume is smaller than 2%, i.e., the transition is slightly discontinuous. In GeSe, the $B16$-$B33$-$B1$ phase sequence observed on heating corresponds to an inversion of the sequence of the two orthorhombic $B16$ and $B33$ structures, with respect to our proposed mechanism. It means that on cooling from the $B1$ structure, the limit $B33$ structure is first stabilized before transforming into $B16$. This picture is confirmed by the first-order and almost second-order characters found, respectively, for the $B1$-$B33$ and $B33$-$B16$ transitions in GeSe. The $R\bar{3}m$ phase found at low temperature in GeTe and SnTe represents a shear deformed $B1$ structure induced by the spontaneous shear components $e_{xy}=e_{xz}=e_{yz}$.

The $B33$-$B2$ or $B16$-$B2$ transformation occurs directly in SnTe and lead chalcogenides with a volume drop ranging

TABLE I. Sequences of temperature- or pressure-induced transitions, related to the $B1$-$B2$ transformation in (Ge, Sn, Pb)- and (Ca, Sr, Ba)-chalcogenides. In column (2), the lower row gives the critical temperature (in Kelvin) or pressure (in GPa), whereas the upper row indicates the corresponding drops in volume $\Delta V/V$. Second (2nd) and first (1st) mean second-order and first-order, respectively. The relevant references corresponding to the materials listed in column (1), are given in column (3).

(1)	(2)	(3)
GeS	$B16$	10,13,19
GeSe	$B16 \xrightarrow[700\ \mathrm{K}]{0.8\%} B33 \xrightarrow[924\ \mathrm{K}]{1\mathrm{st}} B1$	10,13,19
GeTe	$R\bar{3}m \xrightarrow[683\ \mathrm{K}]{2\mathrm{nd}} B1 \xrightarrow[9\ \mathrm{GPa}]{1.4\%} B16$	10,13,19
SnS	$B16 \xrightarrow[878\ \mathrm{K}]{2\mathrm{nd}} B33$	10,11,13,19,61,62
SnSe	$B16 \xrightarrow[807\ \mathrm{K}]{2\mathrm{nd}} B33$	10,11,13,19,61,62
SnTe	$R\bar{3}m \xrightarrow[75\ \mathrm{K}]{2\mathrm{nd}} B1 \xrightarrow[1.8\ \mathrm{GPa}]{2.4\%} B16$	
	$\xrightarrow[25\ \mathrm{GPa}]{} B2$	63
PbS	$B1 \xrightarrow[2.3\ \mathrm{GPa}]{4.3\%} B33 \xrightarrow[22.5\ \mathrm{GPa}]{7\%} B2$	12–14,19
PbSe	$B1 \xrightarrow[4.25\ \mathrm{GPa}]{2.4\%} B33 \xrightarrow[16\ \mathrm{GPa}]{8\%} B2$	12,13,19
PbTe	$B1 \xrightarrow[4.5\ \mathrm{GPa}]{2\%} B16 \xrightarrow[13-16\ \mathrm{GPa}]{4\%} B2$	12,13,19
CaO	$B1 \xrightarrow[65\ \mathrm{GPa}]{11\ \%} B2$	66
CaTe	$B1 \xrightarrow[35\ \mathrm{GPa}]{10.8\%} B2$	67
SrO	$B1 \xrightarrow[36\ \mathrm{GPa}]{13\%} B2$	65
SrS	$B1 \xrightarrow[18\ \mathrm{GPa}]{11.4\%} B2$	70
SrSe	$B1 \xrightarrow[14.2\ \mathrm{GPa}]{10.7\%} B2$	64
SrTe	$B1 \xrightarrow[12\ \mathrm{GPa}]{11.1\%} B2$	67
BaS	$B1 \xrightarrow[6.5\ \mathrm{GPa}]{13.7\%} B2$	68
BaSe	$B1 \xrightarrow[6\ \mathrm{GPa}]{13.9\%} B2$	69
BaTe	$B1 \xrightarrow[4.8\ \mathrm{GPa}]{9\%} B2$	71
InTe	$I4/mcm \xrightarrow[5\ \mathrm{GPa}]{1\mathrm{st}} B1 \xrightarrow[15\ \mathrm{GPa}]{1\mathrm{st}} B2$	24

from 4 to 8 %. These numbers suggest that the intermediate phases, with the orthorhombic symmetries $Pbcm$ and $Cmmm$, assumed in our description of the $B33$-$B2$ transformation, are squeezed within the strong discontinuity occurring at the transformation. Such a discontinuity is inherent to the shear strain (e_{xy}) required to transform the ''latent'' $Cmmm$ symmetry into the $B2$ structure, as noted in Sec. II D.

The two-layer arrangement described by von Schnering and Wiedemeier[11] for the $B33$ structure in SnS and SnSe, and their proposed $B16$-$B33$ displacement mechanism of the bilayers in the [110] direction, is consistent with our description, although the limit character of the $B33$ structure was overlooked by these authors. Another confirmation of our model can be found in the angle-resolved photoemission measurements of the band structure of PbS (Ref. 23) which reveals a maximum along the ΓX (Δ) line of the fcc Brillouin zone. This is in agreement with the phonon softening at the middle of the Δ line that should be observed on approaching the $B1$-$B33$ transition, as resulting from the displacive mechanism assumed for the transition.

For all the alkaline-earth chalcogenides, listed at the bottom of Table I, the $B1$-$B2$ transformation is found to take place directly with a volume drop ranging from 9% in BaTe to 13.7% in BaS. This large discontinuity does not permit, apparently, the stabilization of intermediate structures. Note that it is of the same order than the sum of the volume discontinuities found at the $B1$-$B3$ and $B33$-$B2$ transitions in PbS or PbSe. We have also included in Table I the pressure induced $B1$-$B2$ transition, found in InTe at 15 GPa.[24] InTe displays the remarkable feature that the room pressure tetragonal form, which has the $I4/mcm$ ($Z=8$) ($B37$) structure type, transforms at 5 GPa into the $B1$-type structure, although it constitutes a deformed B2-type structure. The $B2$-$B37$ group-subgroup related transition is induced by an eight-dimensional IR (τ_5 or τ_6 in Kovalev's notation) of the $Fm\bar{3}m$ space group, at the L point ($k_c=(\pi/a,\pi/a,\pi/a)$) of the fcc Brillouin zone.

B. Rare-earth monochalcogenides and monopnictides

The following three distinct sequences of transformations are found for the rare-earth monochalcogenides listed in Table II:

(1) A direct pressure-induced $B1$-$B2$ transformation found in LaTe, GdTe and (Ce, Eu)-(S, Se, Te). The transformation pressures occur between about 7 and 22 GPa with volume drops in the range 4.5– 13.2 %.

(2) A sequence of two pressure-induced transformations $B1 \rightarrow B1 \rightarrow B2$ that has been observed in SmTe and EuO. The isostructural $B1 \rightarrow B1$ transition occurs progressively in SnTe, in the interval 0–6 GPa, and discontinuously in EuO, with a volume drop of about 4%.

(3) A single isostructural $B1 \rightarrow B1$ transition is found in the other rare-earth chalcogenides reported in Table II. It takes place continuously in SmSe, with a small volume drop (e.g., 0.8% in YbSe) or with a large discontinuity as in EuS or EuSe.

The isostructural $B1 \rightarrow B1$ transition is currently interpreted by the $4f \rightarrow 5d$ electron collapse related to the change in valence of the rare-earth ion.[25,26] In the nonstoichiometric rare-earth compounds listed in Table II, the isostructural character of the transition was confirmed by the observation of a critical point of the liquid-gas type (e.g., in $SmS_{1-x}S_x$) or by the existence of two critical points (in $Sm_{1-x}Gd_xS$ and $Sm_{1-x}Y_xS$) bounding the first-order $B1$-$B1$ transition line.[27]

TABLE II. Sequences of pressure induced transitions related to the $B1$-$B2$ transformation in rare-earth chalcogenides and monopnictides. The notation in the columns has the same meaning as in Table I. Cont. or disc. mean that the corresponding isostructural transition is found to take place continuously or with a discontinuous drop in volume. For the nonstoichiometric compounds, a given concentration x has been selected.

(1)	(2)	(3)
LaTe	$B1 \xrightarrow[7\ \mathrm{GPa}]{} B2$	79
CeS	$B1 \xrightarrow[12.5\ \mathrm{GPa}]{4.5\%} B2$	73
CeSe	$B1 \xrightarrow[20\ \mathrm{GPa}]{9\%} B2$	84
CeTe	$B1 \xrightarrow[8.1\ \mathrm{GPa}]{8.5\%} B2$	74
PrTe	$B1 \xrightarrow[9\ \mathrm{GPa}]{11.5\%} B1$	25
SmS	$B1 \xrightarrow[0.65\ \mathrm{GPa}]{12\%} B1$	26
SmSe	$B1 \xrightarrow[0-4.5\ \mathrm{GPa}]{\mathrm{cont.}} B1$	26
SmTe	$B1 \xrightarrow[2-6\ \mathrm{GPa}]{\mathrm{cont.\ or\ disc.}} B1 \xrightarrow[11\ \mathrm{GPa}]{9.1\%} B2$	26
EuO	$B1 \xrightarrow[30\ \mathrm{GPa}]{4\%} B1 \xrightarrow[40\ \mathrm{GPa}]{6.5\%} B2$	26
EuS	$B1 \xrightarrow[21.5\ \mathrm{GPa}]{12.5\%} B2$	26
EuSe	$B1 \xrightarrow[14\ \mathrm{GPa}]{12.8\%} B2$	26
EuTe	$B1 \xrightarrow[10\ \mathrm{GPa}]{13.2\%} B2$	26
GdTe	$B1 \xrightarrow[11.5\ \mathrm{GPa}]{} B2$	79
TmSe	$B1 \longrightarrow B1$	82
TmTe	$B1 \xrightarrow[0.4\ \mathrm{GPa}]{10\%} B1 \xrightarrow[15\ \mathrm{GPa}]{}$ distorted $B1$	25,26
YbO	$B1 \longrightarrow B1$	72
YbS	$B1 \xrightarrow[15-20\ \mathrm{GPa}]{\mathrm{cont.}} B1$	26
YbSe	$B1 \xrightarrow[1-20\ \mathrm{GPa}]{0.8\%} B1$	26
YbTe	$B1 \xrightarrow[15-19\ \mathrm{GPa}]{8\%} B1$	26
$SmS_{1-x}Se_x$	$B1 \xrightarrow[0.97\ \mathrm{GPa}]{x=0.1} B1$	81
$Sm_{1-x}La_xS$	$B1 \xrightarrow[0.4\ \mathrm{GPa}]{x=0.1} B1$	80
$Sm_{1-x}Gd_xS$	$B1 \longrightarrow B1$	27
$TmSe_xTe_{1-x}$	$B1 \xrightarrow[1.5\ \mathrm{GPa}]{x=0.32} B1$	83
$Tm_{1-x}Eu_xSe$	$B1 \xrightarrow{4\%} B1$	87
LaSb	$B1 \xrightarrow[11\ \mathrm{PGa}]{10\%} P4/mmm$	76
CeSb	$B1 \xrightarrow[10\ \mathrm{GPa}]{10\%} P4/mmm$	74
CeBi	$B1 \xrightarrow[13\ \mathrm{GPa}]{6\%} B2+P4/mmm$	77
CeP	$B1 \xrightarrow[10\ \mathrm{GPa}]{3\%} B1 \xrightarrow[19\ \mathrm{GPa}]{10.5\%} B2$	78
CeAs	$B1 \xrightarrow[14\ \mathrm{GPa}]{11\%} B2$	75
NpAs	$B1 \xrightarrow{5.4\ \mathrm{GPa}} P4/mmm \xrightarrow[25-40\ \mathrm{GPa}]{9\%} B2$	86
CeNi	$Cmcm \xrightarrow[125\ \mathrm{K},0.4\ \mathrm{GPa}]{1\mathrm{st}} Cmcm$	30
$Ce_{0.9-x}La_xTh_{0.1}$	$B1 \xrightarrow{0.5-0.7\ \mathrm{GPa}} B1$	85

Let us show that the different experimental situations disclosed in rare-earth chalcogenides can be described by extending the theoretical model proposed in Sec. II. With this aim, we introduce a nonsymmetry breaking order parameter ρ that expresses the change in compressibility of the compound when changing its electronic state, i.e., ρ has two equilibrium values corresponding to the $4f$ and $5d$ states of the rare earth ion. Since ρ is a scalar quantity, all the powers ρ^n are allowed by the symmetry of the initial (parent) $Fm\bar{3}m$ symmetry. On the other hand, the coupling of ρ with the order parameters $\eta(\xi)$ and $\zeta(\xi')$ associated with the $B1$-$B2$ transformation has the form

$$\nu_1 \rho\, \eta^2(\xi) + \nu_2 \rho \zeta^2(\xi'). \tag{3.1}$$

Accordingly, the Landau free energy describing the phase diagram of rare-earth monochalcogenides is

$$F(\eta,\zeta,\rho) = F(\eta,\zeta) + \frac{\alpha}{2}\rho^2 + \frac{\beta}{3}\rho^3 + \frac{\gamma}{4}\rho^4 + \rho(\nu_1\eta^2 + \nu_2\zeta^2), \tag{3.2}$$

where $F(\eta,\zeta)$ is defined by Eq. (2.11). The linear term in the ρ expansion has been discarded by redefining the zero of ρ (with $\rho=0$ in the initial $B1$ structure) and by the subsequent renormalization of the phenomenological coefficients α, β, and γ. Figure 7(a) shows a section of the phase diagram in the (α,a) plane, where α and a are assumed to vary linearly with pressure and temperature. The phase diagram is obtained by a minimization of $F(\eta,\zeta,\rho)$ with respect to ξ,ξ', and ρ, assuming a sixth degree expansion for $F(\eta,\zeta)$, and neglecting the δ coupling between $\eta(\xi)$ and $\zeta(\xi')$. It also assumes a region of stability only for the $B1$, $B33$, and $B2$ phases. One can see that there exists a first-order isostructural transition line between two $B1$ phases, with $\rho=0$ and $\rho\neq 0$, ending at a critical point K. The arrows in Fig. 7(a) represent the thermodynamic paths that have been disclosed experimentally in rare-earth chalcogenides: a $B1\rightarrow B2$ direct first-order transition, a $B1\rightarrow B1\rightarrow B2$ sequence of two first-order transitions, and a $B1\rightarrow B1$ transition that can be slightly or strongly discontinuous depending on the distance to the K-point. Note that the two $B1$ phases merge with the $B2$ phase at the triple point T_1.

The existence of two critical points in the phase diagram of the nonstoichiometric mixtures requires a more elaborated

TABLE III. Sequences of temperature- or pressure-induced transitions, related to the $B1$-$B2$ transformation in alkali and (Ag,Tl) halides, and in alkali metal hydrides. The notation in the columns has the same meaning as in Table I.

(1)	(2)	(3)
NaF	$B1 \xrightarrow{8.9\%,\ 27\ \mathrm{GPa}} B2$	37
NaCl	$B1 \xrightarrow{15\%,\ 30\ \mathrm{GPa}} B2$	92
NaBr	$B1 \xrightarrow{0.57\%,\ 29\ \mathrm{GPa}} B16$	37
NaI	$B1 \xrightarrow{0.51\%,\ 26\ \mathrm{GPa}} B16$	37
KF	$B1 \xrightarrow{10.8\%,\ 3.6\ \mathrm{GPa}} B2$	89
KCl	$B1 \xrightarrow{8.9\%,\ 2\ \mathrm{GPa}} B2$	91
KBr	$B1 \xrightarrow{10.6\%,\ 1.76\ \mathrm{GPa}} B2$	88
KI	$B1 \xrightarrow{8.5\%,\ 1.75\ \mathrm{GPa}} B2$	89
RbF	$B1 \xrightarrow{17.3\%,\ 1.2\ \mathrm{GPa}} B2$	94
RbCl	$B1 \xrightarrow{14.5\%,\ 0.52\ \mathrm{GPa}} B2$	93
RbBr	$B1 \xrightarrow{13.3\%,\ 0.42\ \mathrm{GPa}} B2$	89
RbI	$B1 \xrightarrow{12.8\%,\ 0.35\ \mathrm{GPa}} B2$	89
CsF	$B1 \xrightarrow{10\%,\ 1.97\ \mathrm{GPa}} B2$	89
CsCl	$B2 \xrightarrow{745\%,\ 745\ \mathrm{K}} B1 \xrightarrow{0.53\%,\ 65\ \mathrm{GPa}}$ tetragonal	8,90
CsBr	$B2 \xrightarrow{2\mathrm{nd},\ 53\ \mathrm{GPa}} P4/mmm$	40,41
CsI	$B2 \xrightarrow{2\mathrm{nd},\ 25\ \mathrm{GPa}} Pb2_1m \xrightarrow{2\mathrm{nd},\ 200\ \mathrm{GPa}}$ hcp	42,43
AgF	$B1 \xrightarrow{1.5\%,\ 0.77\ \mathrm{GPa}}$ hex. $\xrightarrow{9.5\%,\ 2.5\ \mathrm{GPa}} B2$	95
AgCl	$B1 \xrightarrow{8\%,\ 7.9\ \mathrm{GPa}} P2_1 \xrightarrow{4\%,\ 13.5\ \mathrm{GPa}} B33 \xrightarrow{4\%,\ 17\ \mathrm{GPa}} B2$	44
TlI	$B33 \xrightarrow[429\ \mathrm{K},0.47\ \mathrm{GPa}]{3.3\%} B2$	96
NaH	$B1 \xrightarrow{6\%,\ 29\text{–}35\ \mathrm{GPa}} B2$	98
KH	$B1 \xrightarrow{13.4\%,\ 4\ \mathrm{GPa}} B2$	97
RbH	$B1 \xrightarrow{11.7\%,\ 2.2\ \mathrm{GPa}} B2$	97
CsH	$B1 \xrightarrow{8.4\%,\ 1.2\ \mathrm{GPa}} B2$	97

interpretation, which refers to the catastrophe theory of phase transitions.[28,29] In this framework, ρ plays the role of an ''internal'' degree of freedom of the system, which does not break the symmetry but may induce a multiplication of the existing singularities. More precisely, ρ induces a nonlinear transformation of the square invariants $\eta^2(\xi)$ and $\zeta^2(\xi)$ which become $\eta^2(\xi)\pm\rho^2$ and $\zeta^2(\xi)\pm\rho^2$. As shown in Ref. 29, such a transformation produces a *doubling* of the critical point K and a reentrance of the $B1$ phase (a ''topological metamorphosis''[29]) which are shown in the phase diagram of Fig. 7(b). The isostructural transition curve K_1K_2 has a shape similar to the first-order transition line bounded by two critical points, found by Aptekar and Tonkov[27] as separating the semiconducting and metallic phases in $Sm_{1-x}Gd_xS$ and $Sm_{1-x}Y_xS$. A similar remarkable $B1$-$B1$ transition line, with two critical points, was also reported in the nonstoichiometric rare-earth compound $CeO_{9-x}La_xTh_{0.1}$, which has been included in Table II.

TABLE IV. Pressure induced $B1$-$B2$ transformation in selected examples of pseudo binary compounds. The corresponding volume drop is not indicated.

(1)	(2)	(3)
KCN	$B1 \xrightarrow{2.2\ \mathrm{GPa}} B2$	102,103
RbCN	$B1 \xrightarrow{0.56\ \mathrm{GPa}} B2$	104,105
NH_4I	$B1 > 270\ \mathrm{K}, 0\text{–}0.3\ \mathrm{GPa} B2$	45,99
NH_4Cl	$B1 > 457\ \mathrm{K}, 0\text{–}0.2\ \mathrm{GPa} B2$	99,100
NH_4Br	$B1 > 400\ \mathrm{K}, 0\text{–}0.2\ \mathrm{GPa} B2$	100,101
KNO_2	$B1 > 350\ \mathrm{K}, 1.1\text{–}1.7\ \mathrm{GPa} B2$	106

The phase diagram of Fig. 7(a) also allows an interpretation of the $B1 \rightarrow B1 \rightarrow B2$ phase sequence observed in the rare-earth monopnictide CeP and of the $B1$-$B2$ transformation in CeAs. The LaSb and CeSb monopnictides show a transformation from the $B1$ to a tetragonally distorted $B2$ structure, with the $P4/mmm$ symmetry ($Z=1$). It obviously corresponds to an intermediate stage between the $Cmmm$ symmetry assumed in our proposed $B33$-$B2$ mechanism, and the B2 structure: the $P4/mmm$ symmetry can be obtained from $B2$ by a ferroelastic deformation with the spontaneous tensile strain $e=e_{xx}+e_{yy}-2e_{zz}$, whereas the $Cmmm$ symmetry results from a further ferroelastic shear deformation e_{xy}. When the c/a ratio strongly differs from 1 (e.g., $c/a \cong 0.82$ in CeSb), the transition to the $B2$ structure may not occur, or take place at much larger pressures as in NpAs. The wide range of coexistence of the tetragonal and cubic ($B2$) structures found in CeBi confirms this interpretation.

In Table I, the isostructural $B33$-$B33$ transition reported in CeNi (Ref. 30) has been included. It has been related to the pressure-induced delocalization of the $4f$ cerium electrons,[30] and can be interpreted on the same basis as the $B1$-$B1$ isostructural transition by assuming a coupling of the compressibility ρ to the order parameter $\eta(\xi)$ associated with the $B1$-$B33$ transition mechanism. Figure 8 shows a (a,α) section through the phase diagram corresponding to the Landau expansion

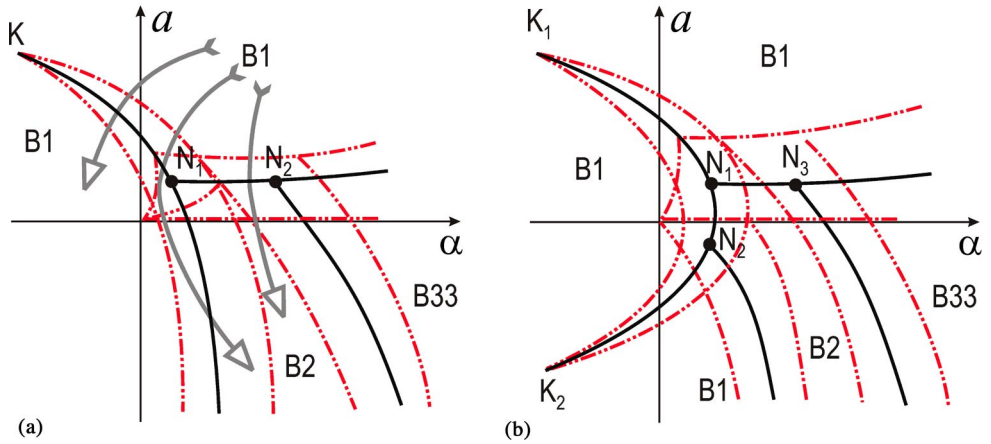

FIG. 7. (a) Phase diagram associated with the Landau free energy defined by Eq. (3.2), in the (a,α) plane. The lines and points have the same meaning as in Fig. 2(b). The isostructural transition line separating the $B1$ phases ends at the critical K point. The arrows show the thermodynamic paths found in rare-earth chalcogenides. (b) Transformation of the phase diagram of (a) when taking into account the doubling of the K singularity, which splits into two critical points K_1 and K_2, as a result of the "topological metamorphosis" described in the text.

$$F[\eta(\xi),\rho]=\frac{a}{2}\eta^2(\xi)+\frac{b}{4}\eta^4(\xi)+\frac{c}{6}\eta^6(\xi)+\frac{\alpha}{2}\rho^2+\frac{\beta}{3}\rho^3$$

$$+\frac{\gamma}{4}\rho^4+\nu\rho\,\eta^2(\xi). \qquad (3.3)$$

The phase diagram contains two distinct regions of stability for the $B33$ structure, which are separated by an isostructural transition line ending at the critical point K.

C. Alkali halides

Three types of phase sequences are found in the alkali halides listed in Table III, which confirm different aspects of our proposed $B1$-$B2$ transformation mechanism. A direct pressure-induced $B1$-$B2$ transformation is observed in 11 members of the family, namely in potassium and rubidium halides, and in NaF, NaCl, and CsF. The transition pressures increase from about 0.35–1.2 GPa in Rb halides to 27–30 GPa in Na-halides. The corresponding volume drops range from about 9 to 15 %. Distinct orientation relations between the $B1$ and $B2$ structures have been reported from x-ray and neutron-diffraction studies. In CsCl, Watanabe *et al.*[8] found the coinciding orientations $[110]_{B2}\|[100]_{B1}$ and $[001]_{B2}\|[011]_{B1}$. An analogous coincidence was disclosed by Blaschko *et al.*[31] in RbI: $[110]_{B2}\|[001]_{B1}$ and $[001]_{B2}\|[110]_{B1}$. In the same compound and in RbCl, RbBr, KF, KCl, KBr, and KI, different orientation relations were observed by Okai[32,33] and Fujiwara *et al.*:[34] $[111]_{B2}\|[100]_{B1}$ and $[100]_{B2}\|[111]_{B1}$. Analogous relations were found by Onodera *et al.*[35] in RbCl. These authors suggested that the multiplicity of orientation relations could be attributed to different external conditions, sample sizes, etc. Figure 9(a) shows a unit cell of the $B2$ structure embedded into a unit cell of the $B1$ structure, consistent with our $B1$-$B2$ mechanism and with Eq. (2.12). It clearly shows *that all the orientation relations* proposed by the different authors *are compatible* with the respective orientations of the $B1$ and $B2$ unit cells, i.e., they can be deduced from the *intrinsic* $B1$-$B2$ transformation mechanism. The coinciding orientations found by Watanabe *et al.*[8] are indicated in the Fig. 9(a), left, whereas the right-hand side of Fig. 9(a) shows the orientations that were found to coincide in Okai's[32,33] studies.

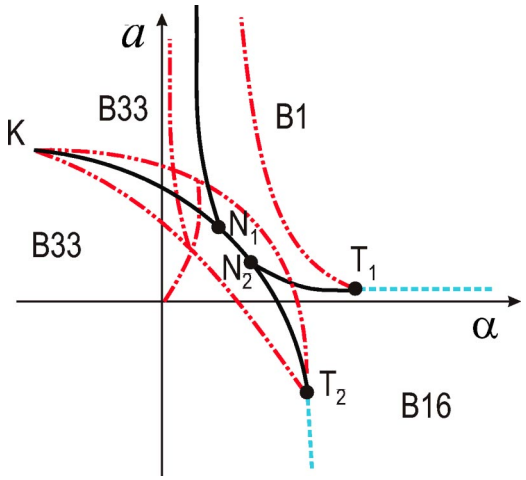

FIG. 8. Phase diagram associated with the Landau free energy defined by Eq. (3.3), in the (a,α) plane. The curves and points have the same meaning as in Fig. 2(b). The isostructural transition line $B33$-$B33$ ends at a critical point K.

In contrast, the fact that analogous, but not identical, orientation relations were found, e.g., by Watanabe *et al.* and Blaschko *et al.*, has to be related to the general property of structural domains at reconstructive transition. Starting from the $B1$ structure, six orthorhombic domains are created at the $B1\rightarrow(B16$ or $B33)$ transition, which transform into one another by the fourfold (three domains) and threefold (three domains) rotations lost at the transition. At the $(B16$ or $B33)\rightarrow B2$ transition, each of the orthorhombic domains will give rise to a differently oriented $B2$ structure. Therefore, the $B1\rightarrow B2$ transformation results into six possible orientations

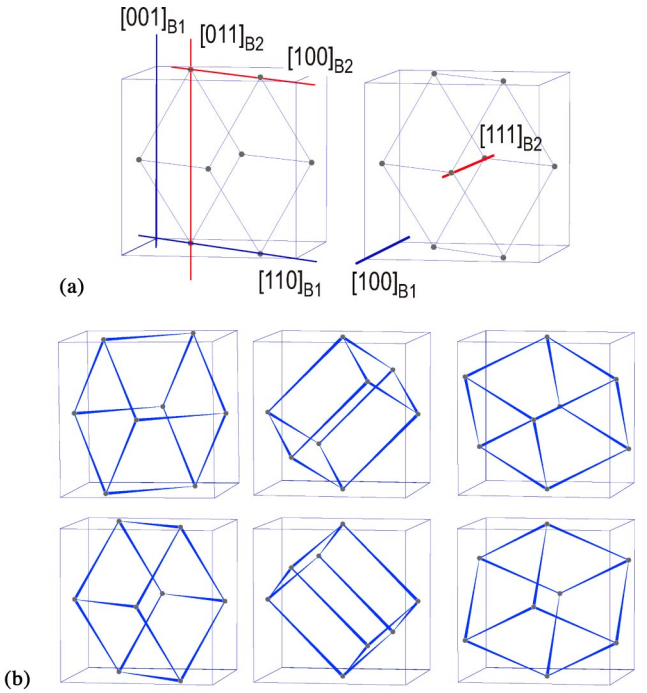

FIG. 9. (a) Orientation relations between the $B1$ and $B2$ structures following the $B1$-$B2$ transformation mechanism are indicated as found by Watanabe *et al.*[8] (left) and Okai[32,33] (right). (b) Orientational domains of the $B2$ structure. Comments on the figure are in the text.

for the cubic $B2$ structure, as shown in Fig. 9(b). Reciprocally, starting from the $B2$ structure, the $B2 \rightarrow B1$ transformation yields six orientational $B1$ domains. In other words, at a reconstructive phase transition, the initial and final structures both display a distribution of domains which reflects the point symmetry of the intermediate structures (here, the orthorhombic mmm symmetry). As a consequence, since our $B1$-$B2$ transformation mechanism implies a coincidence between the $[001]_{B1}$ and $[110]_{B2}$ orientations, it also implies a coincidence between $[100]_{B1}$ or $[010]_{B1}$ orientation with the orientation $[011]_{B2}$ or $[101]_{B2}$. Analogously, the $[110]_{B1}$ direction may coincide with $[100]_{B2}$, $[010]_{B2}$, or $[001]_{B2}$; and $[111]_{B1}$ may coincide with $[100]_{B2}$, $[010]_{B2}$, or $[001]_{B2}$.

In addition to the set of orientational domains, *antiphase* (translational) domains are created at the $B1 \leftrightarrow B2$ transformations. For example, at the $B1 \rightarrow B2$ transition, antiphase domains will form which are deduced from one another by the translations $\vec{t}_1=(a/2,a/2,0)$, $\vec{t}_2=(0,a/2,a/2)$, and $\vec{t}_3=(a/2,0,a/2)$ corresponding to the basic translations of the primitive F unit cell which are "lost" in the $B2$ structure. These antiphase domains may appear as a regular array of stacking faults which have been detected in RbI by Blaschko *et al.*[36] It has to be noted that in their neutron scattering experiments, these authors find traces of an intermediate structure between the $B1$ and $B2$ phases,[31] and of phonon anomalies in frequency and intensity, for the transverse acoustic phonon branch (00ς) corresponding to the Δ line of the fcc Brillouin zone considered in our model.

Another phase sequence $B1 \rightarrow B16$ is observed in NaBr and NaI at 29 and 26 GPa, respectively. This is the first step of the $B1 \rightarrow B2$ transformation mechanism, but no other phase was found in these compounds up to 50 GPa.[37] The small drop in volume ($\sim 0.5\%$) is consistent with the possible second-order character of the $B1 \rightarrow B16$ transition.

CsCl, CsBr, and CsI form a distinct group in alkali halides, the phase sequences of which may illustrate our proposed $B33 \leftrightarrow B2$ mechanism. In the three compounds, the room temperature and pressure phase has the $B2$ structure. In CsCl, the $B2 \rightarrow B1$ temperature-induced transformation takes place at 745 K with a large volume drop of 17%. Two series of contradictory experimental observations were reported for the transformations under pressure. A first set of results using different techniques[38–41] gave an apparently coherent picture with a cubic (B2) to tetragonal continuous transition above, respectively, 65 GPa, 53 GPa, and 38 GPa in CsCl, CsBr, and CsI. Another continuous transition was observed above 56 GPa in CsI, to an orthorhombic phase. The tetragonal phase was suggested to have the CuAuI-type structure corresponding to the space-group symmetry $P4/mmm$ $(Z=2)$. The improper ferroelastic $B2 \rightarrow$CuAuI transition[53] can effectively be of second order and associated with a three-component order parameter transforming as the IR's τ_5 or τ_6, at the X point $[K=(0,\pi/a,0)]$ of the P-cubic Brillouin zone. However, more recent results by Mao *et al.*,[42,43] using synchrotron x-ray diffraction, yield a completely different phase sequence in CsI, which is closely related to our $B33 \leftrightarrow B2$ mechanism. These authors found that above 25 GPa, CsI is orthorhombic and transforms to a hcp structure above 200 GPa.[43] The suggested orthorhombic structure[43] has the same cell-doubled unit cell, with respect to B2, than the $Cmmm$ symmetry assumed in our mechanism to be a shear-strained $B2$ structure. On the other hand, the symmetry "close to" $Pb2_1m$ proposed for the orthorhombic phase is a subgroup of the $Pbcm$ group involved in our $B33 \leftrightarrow B2$ mechanism. In this respect, a verification of the high-pressure "tetragonal" structures disclosed in CsCl and CsBr would constitute an interesting test.

D. (Ag,Tl)-halides and alkali-metal hydrides

In AgCl the pressure-induced $B1$-$B2$ transformation occurs via two intermediate phases[44] having the $B33$ structure and, at lower pressure, a structure that was first suggested to be $B16$,[19] and later the symmetry was proposed to be monoclinic $P2_1$.[44] The 8% drop in volume at the $Fm\bar{3}m \rightarrow P2_1$ transition is effectively in favor of a monoclinic (shear) distortion of the $B1$ structure corresponding to atomic displacements deviating from the $\pm[110]$ directions assumed in our approach. However, symmetry considerations and the structural data reported in Ref. 44 point towards the higher $P2/c$ symmetry, which is more likely than the polar (ferroelectric) $P2_1$ symmetry. In AgF, the $B1$-$B2$ transformation takes place directly above 370 K at 2.5 GPa. Below the preceding temperature, an intermediate structure is stabilized[58] which has been assumed to display the hexagonal inverse NiAs type structure, but the small drop (1.5%) found at the

$B1$-NiAs transition denotes a nonreconstructive transition mechanism and a lower-symmetry structure. Table III also includes TlI that illustrates the last step ($B33 \rightarrow B2$) of the $B1$-$B2$ transformations, and the alkali-metal hydrides (Na, K, Rb, Cs)-H which display a direct pressure-induced $B1$-$B2$ transformation.

E. Pseudobinary compounds

Table IV contains some examples of ammonium halides, univalent cyanides and nitrites, in which the $B1$-$B2$ transformation takes place. For all the listed pseudobinary compounds, the transformation occurs without intermediate structures, and the $B1$ and $B2$ phases are found below the melting line at, respectively, low and high pressures, with a $B1$-$B2$–liquid triple point. Another typical feature of the corresponding phase diagrams[45] is the existence, below the $B1$-$B2$ region of stability, of a number of lower symmetry phases that are group-subgroup related to either the $Fm\bar{3}m$ ($B1$) or to the $Pm\bar{3}m$ ($B2$) symmetries, and, therefore, result from second-order or slightly first-order phase transitions from $B1$ or $B2$. Illustrative examples are the $Pm\bar{3}m \rightarrow P\bar{4}3m$ disorder-order transition in NH_4Cl (Ref. 46) or the ferroelastic $Fm\bar{3}m \rightarrow Immm$ transition in KCN and RbCN,[47] and the $Fm\bar{3}m \rightarrow R\bar{3}m$ transition in KNO_2.[47] The $B1 \rightarrow B2$ transformation mechanism in NH_4Br was investigated by Fraser and Kennedy[48] who found orientational relationships, such as $[010]_{B1} \| [101]_{B2}$, i.e., consistent with the observations reported in alkali halides[8] but involving a different orientational domain. A more surprising result reported by these authors is the change in the shape, from cubic to rhombus shaped, of platelet crystals of $[NH]_4Br$ at the $B1$-$B2$ transformation. This observation is discussed in the following section.

IV. SUMMARY, DISCUSSION, AND CONCLUSION

In summary, a theoretical model has been described in Sec. II for the $B1$-$B2$ transformation which assumes two successive displacive mechanisms corresponding to the $B1$-$B33$ and the $B33$-$B2$ transformations. The second $B33$-$B2$ step also requires the discontinuous onset of a spontaneous shear strain transforming the orthorhombic intermediate structure having $Cmmm$ symmetry into the $B2$ structure. This description follows the general scheme proposed in Refs. 1–6 for the analysis of reconstructive phase transitions, namely, it involves the following:

(1) *Intermediate structures*, the symmetry of which ($Pbnm$ and $Pbcm$) are subgroups of the $Fm\bar{3}m$ ($B1$) and $Cmcm$ ($B33$) initial symmetries,

(2) *Limit structures* ($B33$, $Cmmm$), corresponding to critical displacements, at which the group-subgroup relationship with the initial structures is lost.

However, with respect to the theoretical models proposed for, i.e., the bcc-hcp or bcc-fcc reconstructive transitions,[1–6] the $B1$-$B2$ transformation mechanism appears as more complex, since it requires two distinct sets of displacements and involves intermediate structures which do not correspond to isotropy subgroups of the initial ($B1$) and final ($B2$) structures.

The proposed model has been shown (Sec. III) to provide a consistent interpretation of most of the experimental observations reported for the $B1$-$B2$ transformation. More precisely, we can say the following:

The $B1 \rightarrow B16 \rightarrow B33$ phase sequence is partly or fully realized in the group-IV-elements chalcogenides and in some metal halides. In rare-earth monopnictides, the orthorhombic ($Cmmm$) structure assumed in our proposed $B33$-$B2$ mechanism, is replaced by the supergroup symmetry $P4/mmm$ corresponding to an incomplete shearing of the $B2$ structure.

(2) The different set of orientational relationships found in alkali halides are verified by the relative orientations of the $B1$ and $B2$ structures resulting from our mechanism. Besides, the multiplicity of observed coinciding orientations is explained in terms of the orientational domains, transforming into one another by the cubic symmetry operations lost in the intermediate orthorhombic phases.

(3) The continuous or slightly first-order character found for the $B1 \rightarrow B16$ and $B16 \rightarrow B33$ transitions, support our symmetry analysis of these transitions. This is also the case for the strongly first-order character always found for the $B33 \rightarrow B2$ transition, which may explain the absence of intermediate structures between $B33$ and $B2$, that has been related to the discontinuous character, predicted by symmetry, of the corresponding shear strain. Phonon observations in RbI also confirm our basic symmetry assumption of a soft mode in the fcc-Brillouin-zone Δ direction associated with the full sequence of displacive transitions.

(4) The remarkable features characterizing the isostructural transitions in rare-earth chalcogenides could be interpreted by a coupling of the displacive order-parameters associated with the $B1$-$B2$ transformation, to the change in compressibility related to the valence change of the rare-earth ions.

A number of models were previously proposed for the $B1$-$B2$ transformation. The most cited model by Buerger[7] follows the suggestion by Shoji[49] of a contraction along the [111] cubic direction and a simultaneous expansion at right angles. It is analogous to the Bain-deformation mechanism[50] (bcc-fcc) in which the contraction and expansion occur along and perpendicular to a fourfold cubic direction. Although Buerger's mechanism verifies the increase from sixfold to eightfold atomic coordination, it implies a common [111] direction for the $B1$ and $B2$ structures, which is not observed experimentally. Furthermore, it assumes that the primary transition order-parameter for the $B1$-$B2$ transformation is a pure shear strain, that transforms as the three-dimensional IR τ_7 at the Γ point of the fcc Brillouin zone. This would allow eventual intermediate structures having rhombohedral ($R\bar{3}m$), orthorhombic ($Cmmm$ or $Immm$), monoclinic ($C2/m$), or triclinic ($P\bar{1}$) symmetries, neither of which was observed experimentally.

Two models, based on Buerger's mechanism, have subsequently attempted to correct the preceding deficiencies. As-

suming a martensitic twinning-type mechanism for the $B1$-$B2$ transformation, Fraser and Kennedy[48] deduced the orientation relationships, habit-plane indices and shape deformation associated with different shear components (e_{xz}, $e_{yz,}$, and e_{xy}) involved in the mechanism, assuming coherency stresses between the host and guest phases. This is equivalent to depicting the twinning induced by the transitions to the intermediate structures mentioned here above. In order to fit the orientation relations predicted by Buerger's mechanism, with their own observations in $[NH]_4$Br,[48] Fraser and Kennedy found that a contraction of approximately 40% along [111], and a correlated expansion of not less than 19%, would be necessary. It would lead to a drastic deformation of the crystal shape, which is not observed at the $B1$-$B2$ transformation. The regular change in shape found in some microcrystalline samples of $[NH]_4$Br (Ref. 43) or the volume elongation disclosed in CsCl (Ref. 8) can be well explained by the shear strain which is part of our $B33$-$B2$ transformation mechanism. Gufan and Ternovskii[51] proposed another variant of Buerger's mechanism, which assumes a monoclinic intermediate phase ($C2/m$, $Z=1$) induced by the primary shear strains e_{yz}, e_{xz}, supplemented by the secondary shear (e_{xy}) and tensile ($e_{xx}+e_{yy}-2e_{zz}$) strain components. In terms of atomic displacements, this model can be expressed by a *parallel* shift of the atomic fcc layers (001) along [110], that would lead again to a change in the shape of the crystal from a cubic $B1$ form to an oblique prism form for $B2$, which is not observed experimentally.

A different displacive-type mechanism was proposed by Watanabe *et al.*[8] on the basis of their observations on the temperature-driven $B2 \rightarrow B1$ transformation in CsCl. This mechanism, which is similar to one of the geometrical models proposed by Hyde and O'Keeffe,[52] assumes a shifting of the atoms within the $(110)_{B2}$ layers and a combined shifting of half of these layers along the $[001]_{B2}$ direction. Tolédano and Dmitriev[53] showed that the reversed $B1 \rightarrow B2$ Watanabe mechanism could be expressed by antiparallel displacements of the atoms located in the successive $(001)_{B1}$ planes along the $\pm[110]_{B1}$ directions. It coincides with a soft-mode instability at the zone-boundary X point of the fcc Brillouin zone. The corresponding six-component order parameter yields the sequence of symmetries: $(B1)$ $Fm\bar{3}m \rightarrow Pmmn$ $(Z=2)$ $\rightarrow I4/mmm$ $(Z=1)$ $\rightarrow Pm\bar{3}m$ $(B2)$, with a cell-doubled intermediate orthorhombic phase and the activation of a tensile strain ($e_{xx}+e_{yy}-2e_{zz}$), two features which are not verified experimentally. Watanabe's *et al.* mechanism actually overlooks the two-by-two layers atomic shifting which leads to the observed fourfold $Cmcm$ unit-cell. The symmetry analysis by Stokes and Hatch,[54] who consider maximal isotropy subgroups induced by IR's of the Brillouin-zone boundary, yields the same inadequate intermediate structures proposed by Tolédano and Dmitriev.[53] Similar inadequate results are obtained by Sowa[55] who combines symmetry considerations involving maximal, translational or orientational, subgroups and a geometrical model based on the deformation of a heterogeneous sphere packing.

The fact that the relevant phonon instability associated with the $B1$-$B2$ transformation mechanism is located *inside* the fcc Brillouin-zone, in the middle of the Δ-line, was noted by Christy.[56] From group theoretical consideration, this author proposes the sequence of symmetries: $Fm\bar{3}m \rightarrow Pbnm \rightarrow Cmcm \rightarrow Pbcm \rightarrow Pm\bar{3}m$, which omits, with respect to our proposed description, the limit structure with $Cmmm$ symmetry, and the shear strain e_{xy} required to reach the $B2$ structure. The importance of finding the suitable soft mode instability for understanding the $B1 \rightarrow B2$ mechanism was stressed, by Okai[57] who, however, overlooked the possibility of an instability at a point located inside the fcc Brillouin-zone.

A number of theoretical studies of the $B1$-$B2$ transformations have been recently proposed, based on first-principle calculations .[58–60] These works refer to the direct $B1$-$B2$ transformations that occurs in alkali halides, and do not assume intermediate pathways between the two structures. The main crystallographic models discussed in the present section have also ignored this essential aspect of the $B1$-$B2$ transformation mechanism. Only the recent experimental observations in group-IV-elements chalcogenides have clarified the property of the mechanism to take place via definite intermediate structures. Our analysis has shown that the consecutive stages separating the $B1$ and $B2$ structures are associated with several symmetry breaking mechanisms (order parameters), which makes the $B1$-$B2$ transformation to be indeed one of the most complex examples of reconstructive phase transition.

ACKNOWLEDGMENTS

This work has been supported by the German Science Foundation. One of the authors (P.T.) is pleased to acknowledge the benefit of a Mercator Guest Professorship.

*Permanent address: Groupe ''Structure des matériaux sous conditions extrêmes'' SNBL/ESRF, BP 220, 38043 Grenoble Cedex, France.

†Corresponding author. Email address: knorr@min.uni-kiel.de

[1] P. Tolédano and V. Dmitriev, *Reconstructive Phase Transitions* (World Scientific, Singapore, 1996).

[2] V.P. Dmitriev, S.B. Rochal, Yu.M. Gufan, and P. Tolédano, Phys. Rev. Lett. **60**, 1958 (1988).

[3] V.P. Dmitriev, S.B. Rochal, Yu.M. Gufan, and P. Tolédano, Phys. Rev. Lett. **62**, 844 (1989).

[4] V.P. Dmitriev, Yu.M. Gufan, and P. Tolédano, Phys. Rev. B **44**, 7248 (1991).

[5] O. Blaschko, V. Dmitriev, G. Krexner, and P. Tolédano, Phys. Rev. B **59**, 9095 (1999).

[6] P. Tolédano, G. Krexner, M. Prem, H.P. Weber, and V.P. Dmitriev, Phys. Rev. B **64**, 144104 (2001).

[7] M.J. Buerger, in *Phase Transformations in Solids*, edited by R. Smoluchowski, J.E. Mayers, and W.A. Weyl (Wiley, New York, 1951), p. 183.

[8] M. Watanabe, M. Tokonami, and N. Morimoto, Acta Crystallogr., Sect. A: Cryst. Phys., Diffr., Theor. Gen. Crystallogr. **A33**, 294 (1977).

[9] W.L. Fraser and S.W. Kennedy, Acta Crystallogr., Sect. A: Cryst. Phys., Diffr., Theor. Gen. Crystallogr. **A30**, 13 (1974).
[10] H. Wiedemeier and H.G. von Schnering, Z. Kristallogr. **148**, 295 (1978).
[11] H.G. von Schnering and H. Wiedemeier, Z. Kristallogr. **156**, 143 (1981).
[12] T. Chattopadhyay, H.G. von Schnering, W.A. Grosshans, and W.B. Holzapfel, Physica B **139**, 356 (1986).
[13] T. Chattopadhyay, A. Werner, and H.G. von Schnering, Rev. Phys. Appl. **19**, 807 (1984).
[14] K. Knorr, L. Ehm, M. Hytha, B. Winkler, and W. Depmeier, Eur. Phys. J. B **31**, 297 (2003).
[15] O.V. Kovalev, *Irreducible Representations of the Space Groups* (Gordon and Breach, New York, 1965)
[16] The $\eta(\xi)$ dependence is obtained using the procedure described in Ref. 1, chap. 2. It consists of expressing the $B1$ and $B16$ structures in terms of density waves Ψ_{B1} and Ψ_{B16} taking into account the assumed antiparallel shifting of the critical (001) planes along $\pm[110]$. The increment $\delta\Psi=\Psi_{\mathrm{B1}}-\Psi_{rmB16}$ yields straightforwardly the sinusoidal function defined by Eq. (2.2).
[17] The form of the effective expansion $F[\eta(\xi)]$ is obtained in two steps: (1) by working out the order-parameter invariants of degrees 2,4,6, . . . , which transform as the 12-dimensional IR $\tau_5(k_1^*)$ and, (2) by introducing the equilibrium values $\eta_1=\eta_2=\eta\neq 0, \eta_3=\cdots=\eta_{12}=0$.
[18] The shear strain e_{xy} and the tensile strain e transform respectively as the three-dimensional IR T_2g and the two-dimensional IR, e.g., at the center (Γ) of the fcc-Brillouin zone. Their coupling to the (η_i) order parameter is obtained by standard projection methods.
[19] T. Chattopadhyay, A. Werner, and H.G. von Schnering, Mater. Res. Soc. Symp. Proc. **22**, 93 (1984).
[20] We use the same procedure indicated in Ref. 16 expressing the density waves Ψ_{B33} and Ψ_{Pbcm}.
[21] The $Pm\bar{3}m\rightarrow Cmmm$ proper ferroelastic transition is induced by the zone-center IR T_{2g} of the $Pm\bar{3}m$ space-group, transforming as the shear strains (e_{yz}, e_{xz}, e_{xy}). The $Cmmm$ symmetry is obtained for $e_{yz}=e_{xz}=0$. T_{2g} violates the Landau condition, meaning that a cubic invariant is allowed by symmetry, and that the transition is necessarily discontinuous.
[22] This specific property of reconstructive transition lines is demonstrated in Ref. 1, p. 185.
[23] A. Santoni, G. Paolucci, G. Santoro, K.C. Prince, and N.E. Christensen, J. Phys.: Condens. Matter **4**, 6759 (1992).
[24] T. Chattopadhyay, R.P. Santandrea, and H.G. von Schnering, Physica B **139**, 353 (1986).
[25] A. Chatterjee, A.K. Singh, and A. Jayaraman, Phys. Rev. B **6**, 2285 (1972).
[26] A. Jayaraman, A.K. Singh, A. Chatterjee, and S. Usha Devi, Phys. Rev. B **9**, 2513 (1974).
[27] I.L. Aptekar' and E.Yu. Tonkov, Sov. Phys. Solid State **21**, 110 (1979).
[28] E.I. Kut'in, V.L. Lorman, and S.V. Pavlov, Sov. Phys. Usp. **34**, 497 (1991).
[29] P. Tolédano and A.M. Figueiredo Neto, Phys. Rev. Lett. **73**, 2216 (1994); P. Tolédano and A.M. Figueiredo Neto, V. Lorman, B. Mettout, and V. Dmitriev, Phys. Rev. E **52**, 5040 (1995).
[30] D. Gignoux and J. Voiron, Phys. Rev. B **32**, 4822 (1985).
[31] O. Blaschko, G. Ernst, G. Quittner, G. Pépy, and M. Roth, Phys. Rev. B **20**, 1157 (1979).
[32] B. Okai, J. Phys. Soc. Jpn. **48**, 514 (1980).
[33] B. Okai, J. Phys. Soc. Jpn. **50**, 3189 (1981).
[34] H. Fujiwara, N. Nakagiri, and M. Nomura, J. Phys. Soc. Jpn. **52**, 1665 (1983).
[35] A. Onodera, Y. Nakai, S. Kawano, and N. Achiwa, High Temp.-High Press. **24**, 55 (1992).
[36] O. Blaschko, G. Ernst, G. Quittner, and G. Pépy, Phys. Rev. B **23**, 3017 (1981).
[37] T. Yagi, T. Suzuki, and S.I. Akimoto, J. Phys. Chem. Solids **44**, 125 (1983).
[38] E. Knittle and R. Jeanloz, J. Phys. Chem. Solids **46**, 1179 (1985).
[39] N.E. Christensen and S. Satpathy, Phys. Rev. Lett. **55**, 600 (1985).
[40] K. Asaumi, Phys. Rev. B **29**, 1118 (1984).
[41] A.L. Ruoff, Y.K. Vohra, K.E. Brister, and S. Weir, Physica B **139**, 209 (1986).
[42] H.K. Mao, Y. Wu, R.J. Hemley, L.C. Chen, T.F. Shu, and L.W. Finger, Science **246**, 649 (1989).
[43] H.K. Mao, Y. Wu, R.J. Hemley, L.C. Chen, T.F. Shu, L.W. Finger, and D.E. Cox, Phys. Rev. Lett. **64**, 1749 (1990).
[44] K. Kusaba, Y. Syono, T. Kikegawa, and O. Shimomura, J. Phys. Chem. Solids **56**, 751 (1995).
[45] W. Klement, Jr. and A. Jayaraman, Prog. Solid State Chem. **3**, 289 (1966).
[46] P. Tolédano and J.C. Tolédano, Phys. Rev. B **16**, 386 (1977).
[47] J.C. Tolédano and P. Tolédano, Phys. Rev. B **21**, 1139 (1980).
[48] W.L. Fraser and S.W. Kennedy, Acta Crystallogr., Sect. B: Struct. Crystallogr. Cryst. Chem. **28**, 3101 (1972).
[49] H. Shoji, Z. Kristallogr. **77**, 381 (1931).
[50] E.G. Bain, Trans. AIME **70**, 25 (1924).
[51] Yu.M. Gufan and I.V. Ternovskii, Phys. Solid State **35**, 639 (1993).
[52] B.G. Hyde and M. O'Keeffe, in *Phase Transitions*, edited by L.E. Cross (Pergamon, Oxford, 1973), p. 345.
[53] Ref. 1, p. 243.
[54] H.T. Stokes and D.M. Hatch, Phys. Rev. B **65**, 144114 (2002).
[55] H. Sowa, Acta Crystallogr., Sect. A: Cryst. Phys., Diffr., Theor. Gen. Crystallogr. **A56**, 288 (2000).
[56] A.G. Christy, Acta Crystallogr., Sect. B: Struct. Crystallogr. Cryst. Chem. **49**, 987 (1993).
[57] B. Okai, Physica B **139**, 221 (1986).
[58] A. Martín Pendás, V. Luaña, J.M. Recio, M. Flórez, E. Francisco, M.A. Blanco, and L.N. Kantorovich, Phys. Rev. B **49**, 3066 (1944).
[59] C.E. Sims, G.D. Barrera, N.L. Allan, and W.C. Mackrodt, Phys. Rev. B **57**, 11 164 (1998).
[60] M.A. Blanco, A. Costales, A. Martín Pendás, and V. Luaña, Phys. Rev. B **62**, 12 028 (2000).
[61] T. Chattopadhyay, J. Pannetier, and H.G. von Schnering, J. Phys. Chem. Solids **47**, 879 (1986).
[62] H. Wiedemeier and F.J. Csillag, Z. Kristallogr. **149**, 17 (1979).
[63] J.A. Kafalas and A.M. Mariano, Science **143**, 952 (1963).
[64] H. Luo, R.G. Greene, and A.L. Ruoff, Phys. Rev. B **49**, 15 341 (1994).
[65] Y. Sato and R. Jeanloz, J. Geophys. Res., [Atmos.] **86**, 11 773 (1981).
[66] R. Jeanloz, T.J. Ahrens, H.K. Mao, and P.M. Bell, Science **206**, 829 (1979).

[67] H.G. Zimmer, H. Winzer, and K. Syassen, Phys. Rev. B **32**, 4066 (1985).
[68] S.T. Weir, Y.K. Vohra, and A.L. Ruoff, Phys. Rev. B **33**, 4221 (1986).
[69] S.T. Weir, Y.K. Vohra, and A.L. Ruoff, Phys. Rev. B **35**, 874 (1987).
[70] K. Syassen, Phys. Status Solidi A **91**, 11 (1985).
[71] K. Syassen, Physica B **139**, 277 (1986).
[72] A. Werner, H.D. Hochheimer, A. Jayaraman, and J.M. Léger, Solid State Commun. **38**, 325 (1981).
[73] M. Croft and A. Jayaraman, Solid State Commun. **35**, 203 (1980).
[74] I. Vedel, K. Oki, A.M. Redon, and J.M. Léger, Physica B **139**, 361 (1986).
[75] A. Werner, H.D. Hochheimer, R.L. Mengand, and E. Bucher, Phys. Lett. **97A**, 207 (1983).
[76] J.M. Léger, D. Ravot, and J. Rossat-Mignod, J. Phys. C **17**, 4935 (1984).
[77] J.M. Léger, J. Rossat-Mignod, and O. Vogt, J. Phys. A **46**, 889 (1985).
[78] I. Vedel, A.M. Redon, J. Rossat-Mignod, O. Vogt, and J.M. Léger, J. Phys. C **20**, 3439 (1987).
[79] A. Jayaraman, Bull. Amer. Res. Soc. **24**, 397 (1978).
[80] D.W. Pohl, Phys. Rev. B **15**, 3855 (1977).
[81] A. Jayaraman, P.D. Dermer, and L.D. Longinotti, High Temp.-High Press. **7**, 1 (1975).
[82] D. Debray, A. Werner, D.L. Decker, and M. Loewenhaupt, Phys. Rev. B **25**, 3841 (1982).
[83] H. Boppart and P. Wachter, Mater. Res. Soc. Symp. Proc. **22**, 341 (1984).
[84] J.M. Léger, and A.M. Redon, J. Less-Common Met. **156**, 137 (1989).
[85] J.M. Lawrence, J.D. Thompson, Z. Fisk, J.L. Smith, and B. Batlogg, Phys. Rev. B **29**, 4017 (1984).
[86] U. Potzel, J. Moser, and W. Potzel, J. Magn. Magn. Mater. **63**, 148 (1987).
[87] H. Boppart and P. Wachter, in *Proceeding of 8 th AIRAPT Conference*, edited by C.M. Backman, T. Johannisson, and L. Tegner (Arkitektopia, Uppsala, Sweden, 1982), p. 327.
[88] C.W.F.T. Pistorius, J. Phys. Chem. Solids **26**, 1003 (1965).
[89] C.E. Weir and G.J. Piermarini, J. Res. Natl. Bur. Stand. **68A**, 105 (1964).
[90] K.E. Brister, Y.K. Vohra, and A.L. Ruoff, Phys. Rev. B **31**, 4657 (1985).
[91] W.A. Bassett, T. Takahashi, and J.K. Campbell, Trans. Am. Crystallogr. Assoc. **5**, 93 (1969).
[92] L. Liu and W.A. Bassett, J. Appl. Phys. **44**, 1475 (1973).
[93] S.N. Vaidya and G.C. Kennedy, J. Phys. Chem. Solids **32**, 179 (1971).
[94] G.J. Piermarini and C.E. Weir, J. Chem. Phys. **37**, 1887 (1962).
[95] J.C. Jamieson, P.M. Halleck, and R.B. Roof, J. Phys. Chem. Solids **36**, 939 (1975).
[96] G.A. Samara, L.C. Walters, and D.A. Northrop, J. Phys. Chem. Solids **28**, 1875 (1967).
[97] H.D. Hochheimer, K. Strossner, and W. Hohle, J. Less-Common Met. **107**, L13 (1985).
[98] S.J. Duclos, Y.K. Vohra, and A.L. Ruoff, Phys. Rev. B **36**, 7664 (1987).
[99] A.M. Heyns, K.R. Hirsch, and W.B. Holzapfel, Solid State Commun. **29**, 351 (1979).
[100] C.W.F.T. Pistorius, J. Chem. Phys. **50**, 1436 (1969).
[101] A. Schwake, K.R. Hirsch, and W.B. Holzapfel, J. Chem. Phys. **75**, 2532 (1981).
[102] P.W. Richter and C.W.F.T. Pistorius, Acta Crystallogr., Sect. B: Struct. Crystallogr. Cryst. Chem. **28**, 3105 (1972).
[103] W. Dultz *et al.*, Phys. Rev. B **24**, 1287 (1981).
[104] J.B. Clark and C.W.F.T. Pistorius, Solid State Commun. **7**, 787 (1969).
[105] K. Strössner *et al.*, J. Chem. Phys. **83**, 2435 (1985).
[106] C.W.F.T. Pistorius, High Temp.-High Press. **4**, 77 (1972).